Chemistry
A European
Journal

Chemistry Europe
European Chemical Societies Publishing

Accepted Article

Title: Supramolecular Assembly of Metal Complexes by (Aryl)I···dz2[PtII] Halogen Bond

Authors: Eugene A Katlenok, Matti Haukka, Oleg V Levin, Antonio Frontera, and Vadim Yurievich Kukushkin

To be cited as: *Chem. Eur. J.* 10.1002/chem.202001196

Link to VoR: https://doi.org/10.1002/chem.202001196

WILEY-VCH

10.1002/chem.202001196

Supramolecular Assembly of Metal Complexes by (Aryl)I···d_z^2[Pt^{II}] Halogen Bond

Eugene A. Katlenok[a], Matti Haukka[b], Oleg V. Levin[a], Antonio Frontera[c]*, Vadim Yu. Kukushkin[a], [d]*

[a] Dr. Eugene A. Katlenok, Dr. Oleg V. Levin, Prof. Dr. Vadim Yu. Kukushkin
Institute of Chemistry
Saint Petersburg State University
Universitetskaya Nab. 7/9, 199034 Saint Petersburg, Russian Federation
E-mail: v.kukushkin@spbu.ru
[b] Prof. Dr. Matti Haukka
Department of Chemistry
University of Jyväskylä
P.O. Box 35, FI-40014 Finland
[c] Prof. Dr. Antonio Frontera
Department de Química
Universitat de les Illes Balears
Crta. de Valldemossa km 7.5, 07122, Palma, de Mallorca, Baleares, Spain
E-mail: toni.frontera@uib.es
[d] Prof. Dr. Vadim Yu. Kukushkin
Laboratory of Crystal Engineering of Functional Materials
South Ural State University, 76, Lenin Av., Chelyabinsk, 454080, Russian Federation

Supporting information for this article is given via a link at the end of the document.

Abstract. The theoretical data for the half-lantern complexes $[Pt(C^N)(\mu\text{-}S^N)]_2$ (**1**–**3**; C^N is cyclometalated 2-Ph-benzothiazole; S^N is 2-SH-pyridine **1**, 2-SH-benzoxazole **2**, 2-SH-tetrafluorobenzothiazole **3**) indicate that the Pt···Pt orbital interaction leads to an increment of the nucleophilicity of the outer d_z^2-orbitals to provide assembly with electrophilic species. **1**–**3** were co-crystallized with bifunctional halogen bond (XB) donors to give adducts (**1**–**3**)$_2$·(1,4-diiodotetrafluorobenzene) and infinite polymeric [**1**·1,1'-diiodoperfluorodiphenyl]$_n$. X-ray crystallography revealed that the supramolecular assembly is achieved via (Aryl)I···d_z^2[Pt^{II}] XB between iodine σ-holes and lone pairs of the positively charged (Pt^{II})$_2$ centers, acting as nucleophilic sites. The polymer includes a curved linear chain ···Pt$_2$···I(arene^F)I···Pt$_2$··· involving XB between iodines of the perfluoroarene linkers and (Pt^{II})$_2$ moieties. The ^{195}Pt NMR, UV-vis, and CV studies indicate that XB is preserved in CH(D)$_2$Cl$_2$ solutions.

Introduction

Halogen bonding (XB) is an interdisciplinary area of rapidly rising interest as collaterally reflected in a substantial amount of relevant reviews and book chapters. The recently published surveys were devoted to theoretical approaches to XB[1-2] and also roles of XB in supramolecular chemistry,[3-9] catalytic transformations,[10] synthetic coordination chemistry,[11-16] polymer chemistry,[17] drug discovery,[18-21] and, eventually, to the involvement of XB in human function.[22-23] Together with other weak interactions such as hydrogen-,[24] chalcogen-[25-27] or pnictogen[28] bonding, metallophilic,[29] and π–π interactions,[30] XB has been recognized as a useful tool for design of supramolecular systems and, in particular, for crystal engineering.

In the vast majority of XB studies, organic iodine species R^{EWG}I featuring electron withdrawing group R^{EWG} were applied as σ-hole (h) donors, while commonly used accepting centers included electronegative hetero-atoms bearing lone pair(s) (LP) such as halogens and

10.1002/chem.202001196

also O, S, N, P and other atoms, electron-donating C (e.g. –C≡C⁻, or π-system in alkene, alkyne, arene). Incomparably less common is the application of d_z^2-orbital donating positively charged metal centers as XB acceptors; a metal can act as XB acceptor if it contains at least one LP, which could interact with empty σ*-orbital(s) of appropriate XB donor(s). Although examples of metal-involving XB are quite rare, they still have been reported for Ni^{II}, Rh^{I}, Pd^{II}, Pt^{II}, Au^{0}, and Au^{I}.[31-36] All these XBs with the metals were observed in simple (often 1:1) adducts, while assembly or supramolecular design via $R^{EWG}X\cdots d_z^2$[M] XB of positively charged d_z^2[M] centers and σh-X-donating species has never been performed and this task was challenging.

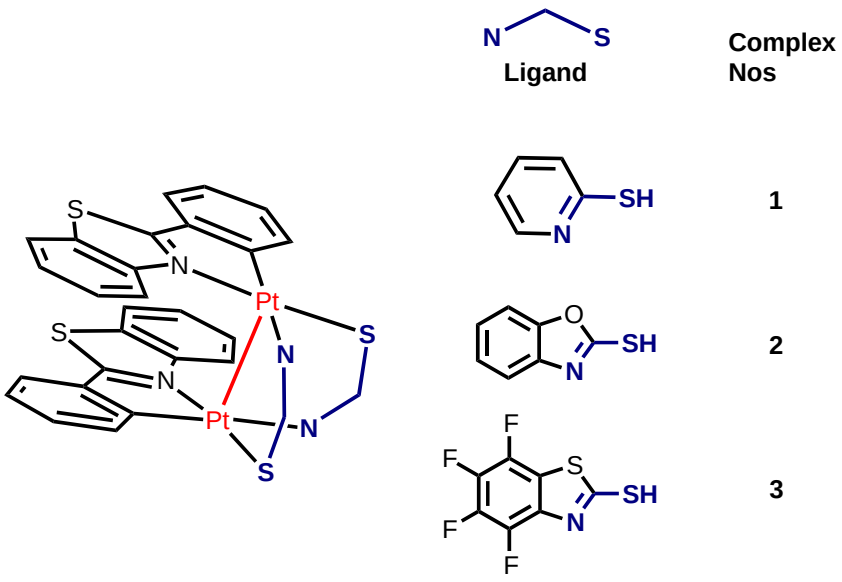

Figure 1. Half-lantern complexes as XB acceptors and complex numbering.

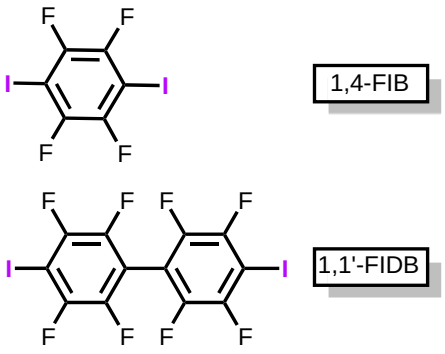

Figure 2. Bifunctional XB donors employed for this study.

For the current work we addressed the known half-lantern complexes[37-38] (**Figure 1**) featuring the bridging (thio)azaheterocyclic ligands of the rigid geometry. These ligands serve as molecular staples bringing two metal centers and stimulating repulsive metal–metal interactions between d_z^2-orbitals of two Pt^{II} centers. This repulsion, as we expected, should lead to the increased nucleophilicity of the outer orbitals. Consequently, metal centers with the increased nucleophilicity of the outer $d_z^2Pt^{II}$ orbitals might behave as synthons for the XB assembly involving metal centers. As σh donor we employed two symmetric iodoperfluoroarenes (**Figure 2**) that are rather commonly applied for XB crystal engineering (for statistics of their usage see our recent works[39-40]).

Results and Discussion

XRD and MEP data for the XB donors and acceptors. The single-crystal X-ray diffraction (XRD) studies of parent half-lanterns **1**–**2** (CSD codes: RORTEZ and JACTAL, correspondingly) and **3** (this work; the Supporting Information) revealed that their structures consist of the centrosymmetric dimeric platinum complexes, where both Pt^{II} centers exhibit a square-planar environment. The Pt–Pt distances (2.8515–2.9942 Å) in each Pt_2 core are less than the sum of Bondi van der Waals radii ($\sum R_{vdW}$; 3.5 Å) and this comparison favors the chemical bond between the metal centers[41-48] (**Table S1**, the Supporting Information). A simplified molecular orbital approach indicates that the axial interactions of the metal centers led to the d_z^2-orbitals overlap to give bonding ($d\sigma$) and antibonding ($d\sigma^*$) orbitals. The antibonding character of HOMO of the dinuclear d^8–d^8 complexes may explain why does the oxidation leads to enhanced Pt–Pt bonding on going from $(Pt^{II})_2$ (2.798–2.994 Å; **Table S1**) to $(Pt^{III})_2$ (2.518–2.680 Å).[49]

To get a preliminary estimate of the possibility of electrostatic interaction between half-lantern complexes **1**–**3** (**Figure 3** for **2**–**3**; **Figure 5***b* for **1**) and bifunctional XB donors 1,4-FIB

10.1002/chem.202001196

and 1,1'-FIDB (**Figure 4**), we computed the MEP surfaces for all these species.

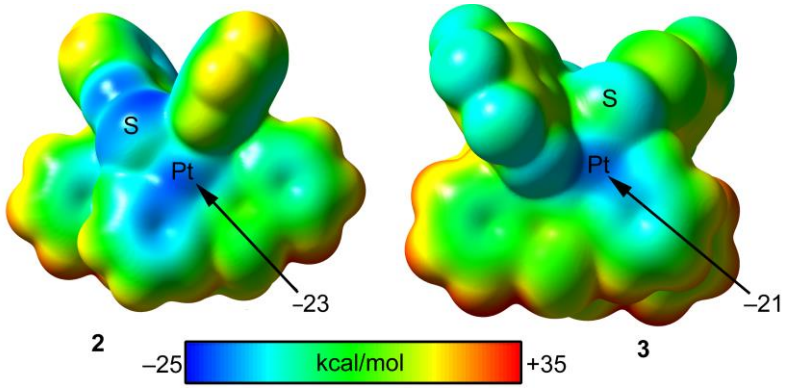

Figure 3. MEP surfaces (0.001 a.u.) of **2** and **3** at the PBE0-D3/def2-TZVP level of theory. The values at selected points of the surfaces are given in kcal/mol. The color scheme is taken from Politzer's work (Ref.[50]).

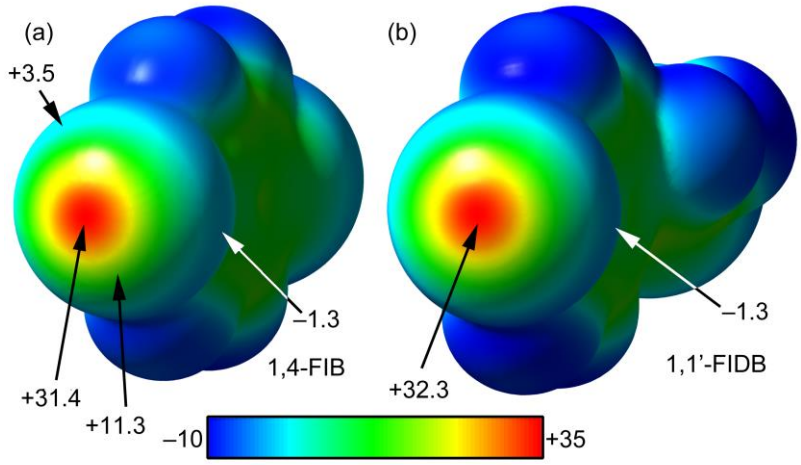

Figure 4. MEP surfaces (0.001 a.u.) of 1,4-FIB (*a*) and 1,1'-FIDB (*b*) at the PBE0-D3/def2-TZVP level of theory; the values at σh are given in kcal/mol. The color scheme is taken from Politzer's work (Ref.[50]).

In addition, and for comparison purposes, we also computed the MEP surface of two additional species: (*i*) a mononuclear model (**Figure 5***a*) of the complex in order to analyze the effect of the Pt···Pt interaction upon the MEP value at the Pt center and (*ii*) adduct (**1**·1,1'-FIDB) (**Figure 5***c*) in order to investigate the influence of XB upon the MEP of the Pt center

10.1002/chem.202001196

located at the opposite side. In **1**–**3**, the MEP values of Pt^{II} atoms are significantly negative, ranging from –28 to –21 kcal/mol. Complex **1** exhibits the largest absolute value of MEP at the Pt^{II} center confirming the ability of this metal center to act as an electron rich atom or, in other words, a Lewis base. In **3**, the MEP value at the Pt^{II} atom is the lowest among the three species due to the strong electron withdrawing effect of the F atoms. It is noteworthy that compared to **1**, its mononuclear model (**Figure 5***a*–*b*) presents a lower value of MEP (–26.3 kcal/mol) thus confirming the fact that the Pt···Pt orbital interaction leads to an increment of the nucleophilicity of the outer d_z^2-orbitals. Moreover, the MEP value at the Pt atom in adduct (**1**·1,1'-FIDB) is significantly smaller compared to **1** (–21.3 kcal/mol) thus revealing that the formation of XB interaction at one Pt atom reduced the nucleophilicity of the other Pt center.

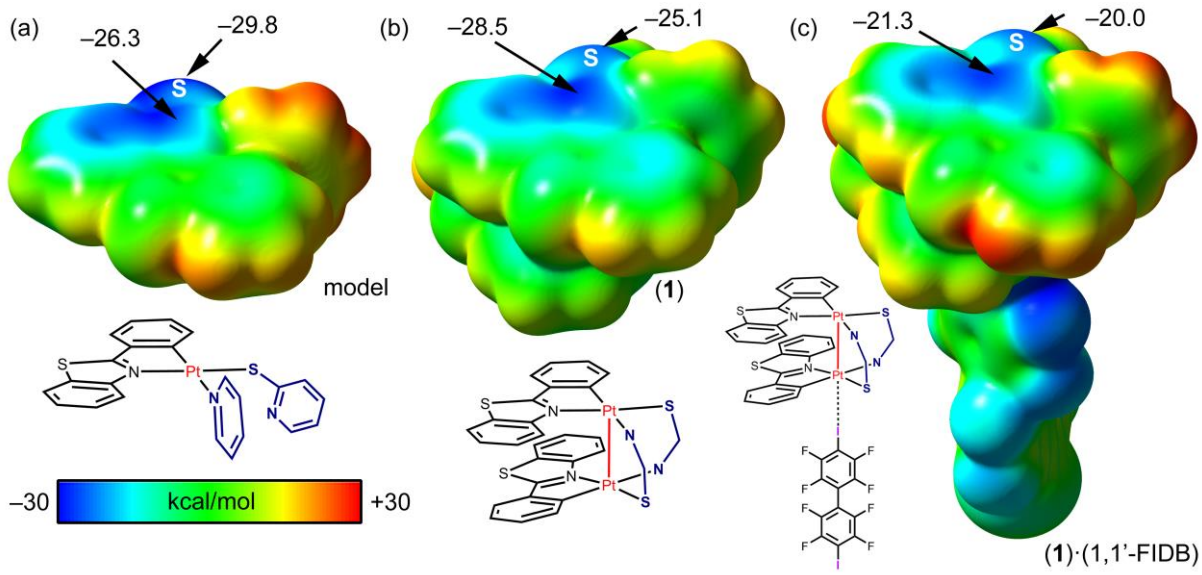

Figure 5. MEP surfaces (0.001 a.u.) of a mononuclear model (*a*), (**1**) (*b*) and (**1**)·(1,1'-FIDB) (*c*) at the PBE0-D3/def2-TZVP level of theory; the values at the Pt and S-atoms are given in kcal/mol. The color scheme is taken from Politzer's work (Ref.[50]).

As expected, both 1,4-FIB and 1,1'-FIDB exhibit large and deep σh (+31.4 and +32.3 kcal/mol, respectively). The value at the negative belt (dark blue color) at the I atom is very small in both compounds (–1.3 kcal/mol) and that the σh is extended up to the light blue

colored region around the I-atom thus evidencing the large size of the σh. The obtained MEP results clearly indicate that the electrostatic interaction between d_z^2Pt^{II} and σh of the XB donors are favorable from electrostatic viewpoint.

Assembly by (Aryl)I···d_z^2[Pt^{II}] XB. Adducts **1**$_2$·1,4-FIB·2CH_2Cl_2, **2**$_2$·1,4-FIB, **3**$_2$·1,4-FIB·2C_6H_6, and polymeric [**1**·1,1'-FIDB]$_n$ (or, taking into account disordered cyclohexane, [**1**·1,1'-FIDB]$_n$·4.77C_6H_{12}) were obtained by the crystallization of **1**–**3** with 1,4-FIB and 1,1'-FIDB at 2:1 and 1:1 molar ratios, respectively, from CH_2Cl_2 (**1**$_2$·1,4-FIB·2CH_2Cl_2 and **2**$_2$·1,4-FIB), CH_2Cl_2–benzene (**3**$_2$·1,4-FIB·2C_6H_6), or CH_2Cl_2–cyclohexane ([**1**·1,1'-FIDB]$_n$·4.77C_6H_{12}) at 20–25 °C. In the following section, the solvated adducts for simplicity are given without solvent molecules, viz. (**1**–**3**)$_2$·1,4-FIB and [**1**·1,1'-FIDB]$_n$.

Table 1. Comparison of the C–I and Pt–Pt bond distances in the adducts with those in separate components; solvent molecules in the structures are omitted for simplicity.

Structure	*d*(Pt–Pt), Å	*d*(C–I), Å
1$_2$·1,4-FIB	2.8518(2)	2.131(4)
[**1**·1,1'-FIDB]$_n$	2.8516(3) 2.8503(3)	2.124(6) 2.124(6) 2.145(7) 2.133(6)
1 (CSD code: RORTEZ)	2.8764(4)	
2$_2$•1,4-FIB	2.9503(3)	2.123(5)
2 (CSD code: JACTAL)	2.9942(4)	
3$_2$•1,4-FIB	2.9035(4) 2.9140(5)	2.080(9) 2.094(8)
3 (this work)	2.9779(5) 2.9437(5)	
1,4-FIB (CSD code: ZZZAVM02)	–	2.0746(10)
1,1'-FIDB*	–	2.0655(2)

*Our unpublished data.

In all these structures, we observed the decrease of Pt–Pt distances as compared to the parent complexes (by 0.02–0.06 Å) accompanied with the increase of the I–C bond length with respect to 1,4-FIB and 1,1'-FIDB (by 0.06–0.08 Å; **Table 1**). These data along with the MEP data (see above) located on the σh of the I atom indicate that I···Pt short contacts are due to

10.1002/chem.202001196

XB in accord with the IUPAC criteria for Type II XB interactions;[51] the iodine atom from 1,4-FIB acts as a σh donor, which interacts with a d_z^2-orbital of a platinum(II) center.

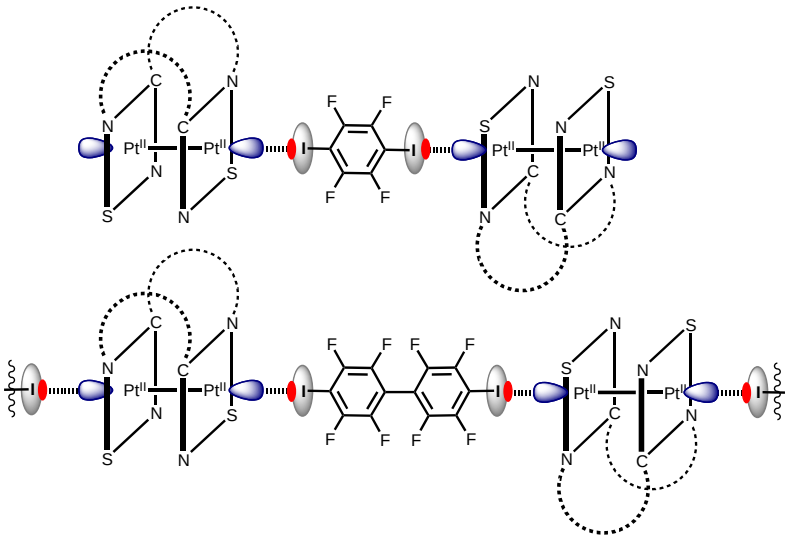

Figure 6. Schematic representation of noncovalent bonding in the 1,4-FIB (*top*) and 1,1'-FIDB (*bottom*) adducts.

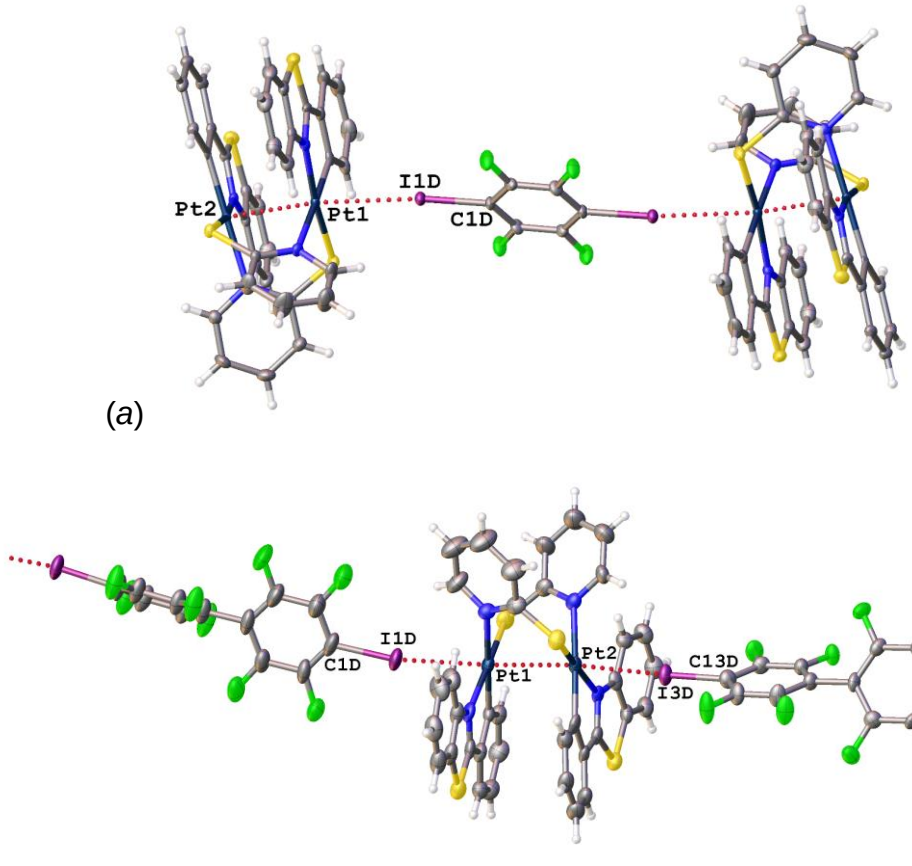

Figure 7. Fragments of the crystal structure of **1**$_2$·1,4-FIB (*a*) and [**1**·1,1'-FIDB]$_n$ (*b*). Contacts

10.1002/chem.202001196

shorter than $\sum R_{vdW}$ are given by dotted lines and thermal ellipsoids are shown at the 50% probability level.

In **1**$_2$·1,4-FIB (**Figure 6** and **Figure 7***a*) and [**1**·1,1'-FIDB]$_n$ (**Figure 6** and **Figure 7***b*), the C–I···Pt contacts comprise 83–86% of $\sum R_{vdW}$, respectively, while the corresponding ∠C–I···Pt are close to 180° (∠C–I···Pt 174.11(13) for **1**$_2$·1,4-FIB and 176.0(2), 177.6(2), 167.75(19)° for [**1**·1,1'-FIDB]$_n$. This structure of [**1**·1,1'-FIDB]$_n$ can be viewed as a curved linear chain ···Pt$_2$···I(arene^F)I···Pt$_2$··· involving XB between iodines of the perfluoroarene linkers and (Pt^{II})$_2$ centers. One Pt$_2$ unit is linked by the neighboring I of 1,1'-FIDB with rather long Pt···I distance (3.1264(4), 3.1380(6) Å), whereas the other separation is shorter (3.0892(6), 3.0979(4) Å).

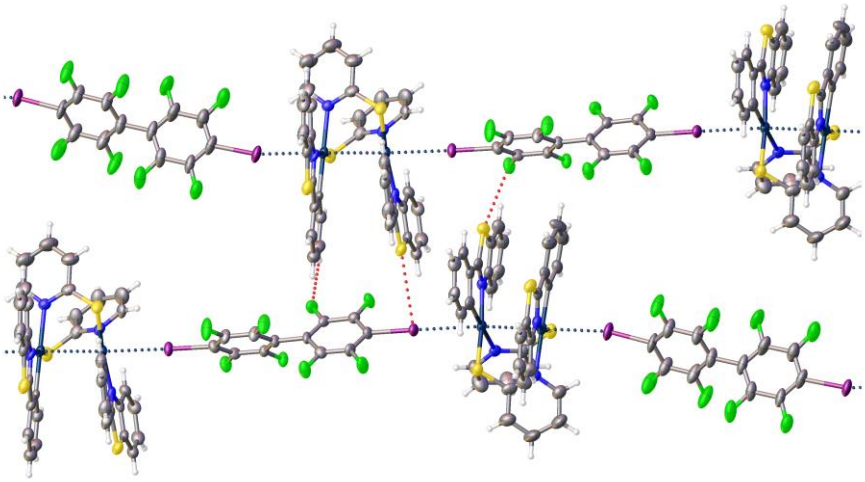

Figure 8. A fragment of Pt–Pt chains [**1**·1,1'-FIDB]$_n$. Contacts shorter than $\sum R_{vdW}$ are given by dotted lines and thermal ellipsoids are shown at the 50% probability level.

In the structure of [**1**·1,1'-FIDB]$_n$, two chains are linked to each other via C−S···I, double C−S···F contacts, and also by hydrogen bonds (HBs). The contact C−S···I (*d*(S···I) 3.7235(13) Å; **Figures 8** and **S2**) is shorter than $\sum R_{vdW}$ (I + S = 3.780 Å),[52] whereas ∠C–S···I is 161.1(3)° and ∠S···C–I is 84.64(15)° thus favoring chalcogen bonding (ChB).[53-54] The second type contact between the 1,1'-FIDB and the heterocyclic S atoms is C−S···F (*d*(S···F) = 3.240(3)

Å)[55] is less than $\sum R_{vdW}$ (S + F) = 3.27 Å),[52] while ∠C–S···F is 166.4(2)°; these values also favor ChB.[53-54]

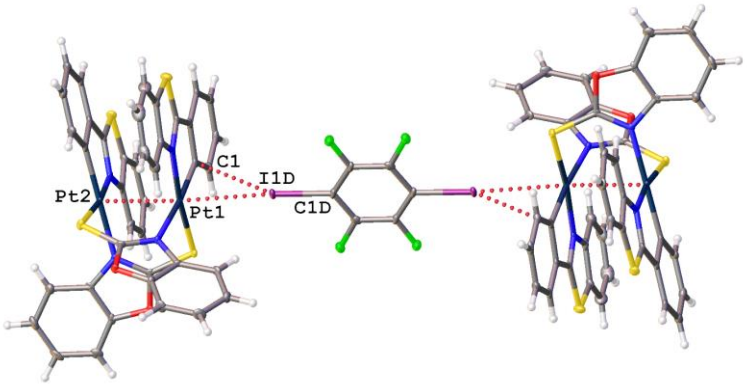

Figure 9. A fragment of the crystal structure of $\mathbf{2}_2$·1,4-FIB. Contacts shorter than $\sum R_{vdW}$ are given by dotted lines and thermal ellipsoids are shown at the 50% probability level.

In the structure of $\mathbf{2}_2$·1,4-FIB (**Figure 9**), each iodine atom of 1,4-FIB interacts with two Pt_2 centers and, in addition, with the C atom of the cyclometalated ligand; the distances (d(I···Pt) 3.2494(4) and d(I···C) 3.311(5) Å) are less than the corresponding $\sum R_{vdW}$ (I + Pt = 3.73; I + C = 3.68 Å, comprising 87 and 90% of $\sum R_{vdW}$) and both contact angles are not much different from 160° (∠(C–I···Pt) 174.28(16) and ∠(C–I···C) 150.16(18)°). Consideration of these data indicates the presence of the I···η^2(Pt–C) bifurcated metal-involving XB; the Pt–C moiety can be viewed as an integrated XB acceptor. This intricate combination of interactions is further analyzed and confirmed by the QTAIM and NCIplot analyses (see later).

10.1002/chem.202001196

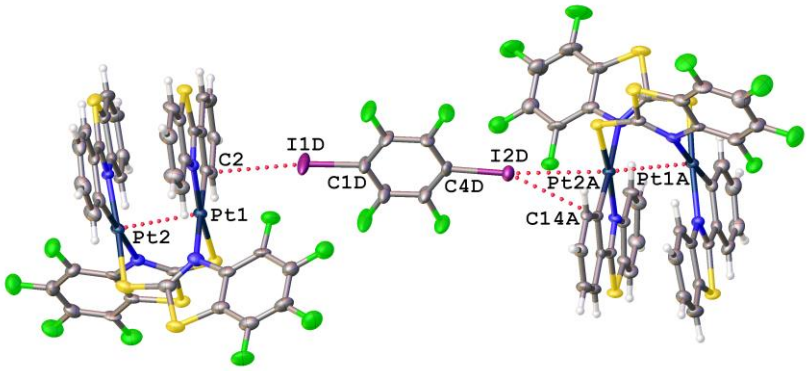

Figure 10. A fragment of the crystal structure of **3**$_2$·1,4-FIB. Contacts shorter than $\sum R_{vdW}$ are given by dotted lines and thermal ellipsoids are shown at the 50% probability level.

The structure of **3**$_2$·1,4-FIB contains two crystallographically independent complex molecules (**Figures 10, S3**). On the one hand, I atom of 1,4-FIB forms a short contact with the C atom (C2) *d*(I···C) 3.213(8) Å, ∠(C–I···C) 165.5(3)°) of the cyclometalated ligand, on the other hand, it is bonded to both C and Pt atoms; the distances (*d*(I···Pt) 3.4741(8) and *d*(I···C) 3.437(8) Å) are less than the corresponding $\sum R_{vdW}$ (I + Pt = 3.73; I + C = 3.68 Å; 93 and 93% from $\sum R_{vdW}$) and both contact angles are rather close to 160° (∠(C–I···Pt) 168.6(2) and ∠(C–I···C) 168.2(3)°) (**Table 1**).

The Hirshfeld surface analysis. The molecular Hirshfeld surface[56-59] represents an area where molecules come into contacts, and its analysis gives the possibility of an additional insight into the nature of intermolecular interactions in the crystal state. The obtained Hirshfeld surface plots (**Figures S4, S5**, **S10**) display a surface where contacts shorter than $\sum R_{vdW}$ have negative values of d_{norm} and appear as conspicuous red spots, while contacts longer than $\sum R_{vdW}$ have positive values of d_{norm} and are mapped in blue. The analysis for all four adducts expectedly indicates the domination of the contacts involving hydrogens). Other important contacts include I···Pt (8%; the contribution is indicated by the contribution of contact of I with all atoms) with involvement of I···C (12% for **1**$_2$·1,4-FIB, 8% for **1**$_2$·1,4-FIB and 15% for [**1**·1,1'-FIDB]$_n$) contacts. For **2**$_2$·1,4-FIB, we found a reduced contribution of I···Pt (3%) and increased

contribution of I···C (24%) contacts; a bright red spot from the F···I (12%) contacts was also detected.

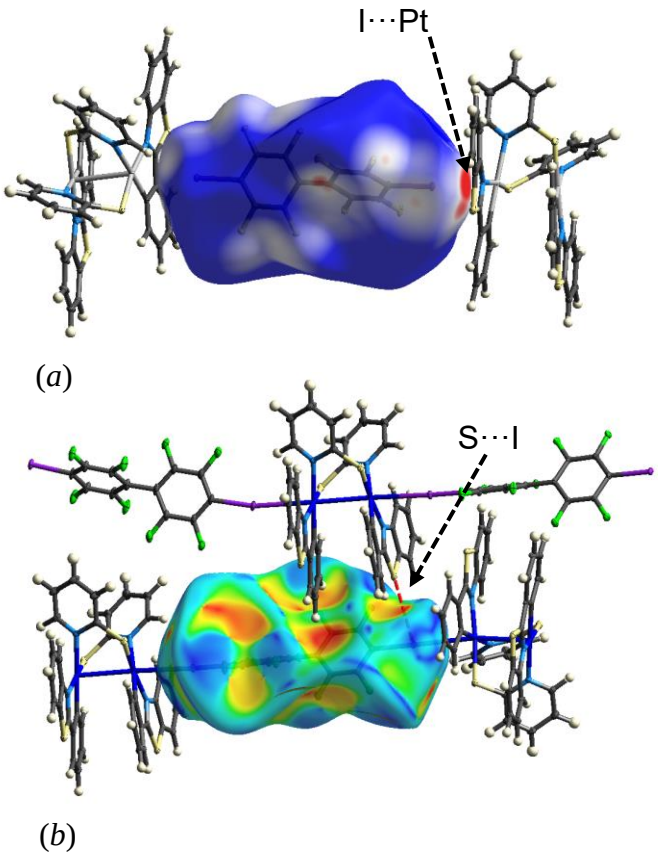

Figure 11. The Hirshfeld surfaces for [**1**·1,1'-FIDB]$_n$. (*a*) mapped with d_{norm} over the range –0.20 (*red*) to 1.00 (*blue*); (*b*) shape index (S), mapped from –1.0 (concave hollows; red) → 0.0 (minimal saddle; green) → +1.0 (convex bumps; blue).

According to the crystallographic data, the one-dimensional chains for [**1**·1,1'-FIDB]$_n$ are interconnected not only by HB, but also by the ChB C−S···I (*d*(S···I) 3.7235(13) Å). The contact found was analyzed using a Hirshfeld surface mapped to a shape index; the latter better highlights intermolecular contacts,[60-62] in particular the S···I contact (see above and **Figure 11**). The fingerprint plot and percentage contributions of each interaction to the Hirshfeld surface are depicted in **Figures S6**–**S9**. Although these data are useful to support our XRD considerations regarding the assembly via I···Pt contacts, the Hirshfeld surface analysis does not answer the question of the energies of these contacts and, therefore, the

DFT calculations should be further performed.

Theoretical study of XB. We computed the interaction energies of supramolecular dimeric complexes (**1**)$_2$–(**2**)$_2$·1,4-FIB and (**1**)·(1,1'-FIDB) (**Figure 12**) retrieved from the X-ray structures and found that these energies are moderately strong and in agreement with the obtained MEP data (see above). We studied the two types of XB in the adduct of **3**$_2$·1,4-FIB (**Figure 10**), namely with the Pt center and with the π-system (**Figure 12***b*,*c*) and the latter is weaker than the former, as expected taking into consideration the MEP surface.

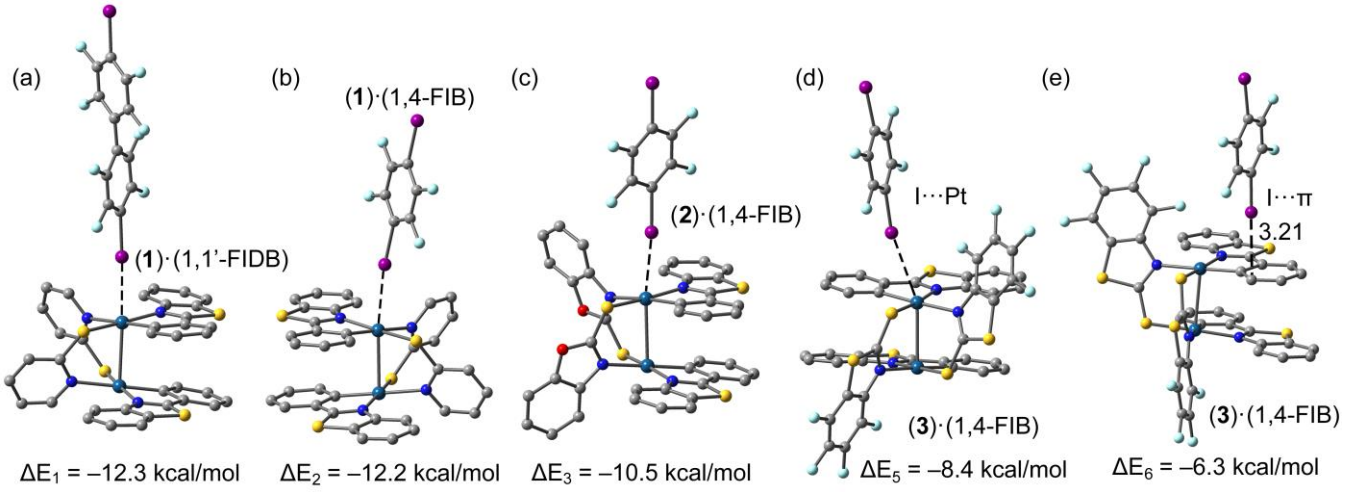

Figure 12. The complexes and the associated binding energies at the PBE0-D3/def2-TZVP level of theory; distances in Å.

The supramolecular dimeric complexes were studied using the QTAIM analysis (**Figures S11**–**13)**. The distribution of bond critical points (CPs) and bond paths reveals that in the three adducts, the I atom is linked to the Pt metal center and also to an H-atom of the aromatic ligand. In (**3**)$_2$·1,4-FIB, the I is connected to the Pt^{II} center and also to the F-atom of the fluorinated ligand. In (**3**)$_2$·1,4-FIB, where the I points to the π-system, the interaction is characterized by a single bond CP and bond path connecting the I to one C atom of the ring. In **Table 2**, we summarize the values or ρ(r), electronic potential energy density [V(r)] and electronic kinetic energy densities [G(r)] at the critical points labeled in (**Figures S11–S13**). The energy contributions of each interaction based on the AIM parameters (E = 0.5V(r) for

HB[63] and E = 0.556V(r)[64] for XB] are also included. As can be inferred from inspection of the obtained data, the XB is the dominating interaction and that the HB is weak (1–2 kcal/mol). In accord with the MEP analysis, the XB contribution is larger **1** (–8.7 and –7.6 kcal/mol) than in the rest of complexes. It is noteworthy that the I···F interaction also contributes to the binding energy in 2.1 kcal/mol, thus indicating that this interaction is attractive in its nature. In fact, the F atom of the ligand points to a region of the I-atom where the MEP value is positive. As previously commented (**Figure 4**) the σh at the I-atom is very extended and the negative belt is very thin and insignificant. In general, the energies predicted by the QTAIM parameters are smaller than those using the standard PBE0 binding energies probably because the QTAIM does not take into account long-range interactions that also participate in the stabilization of the supramolecular assembly. Finally, it is worthy to comment that the behavior of the energy densities (V_r and G_r) at the bond CP that interconnects the Pt atoms, denoted as CP(Pt···Pt) in **Figure S11**. That is, the energy density values are significantly smaller in (**1**)–(**2**) compared to the adducts, thus revealing that the Pt···Pt interaction is reinforced upon complexation, thus supporting the electron-withdrawing ability of the I-atom.

Table 2. QTAIM ρ(r), V(r) and G(r) parameters at the bond CPs labeled is **Figures S11**–**13** in a.u. and predicted energies for each interaction using the electronic potential energy densities in kcal/mol.

Supramolecular cluster	CP	ρ(r)	V(r)	G(r)	E (QTAIM)	E (PBE0)
(**1**)·(1,1'-FIDB)	CP6 (XB) CP7 (HB) CP(Pt···Pt)	0.0213 0.0052 0.0415	–0.0250 –0.0037 –0.0514	0.0233 0.0044 0.0428	–8.7 –1.2	–12.3
(**1**)$_2$·1,4-FIB	CP8 (XB) CP9 (HB) CP(Pt···Pt)	0.0194 0.0059 0.0411	–0.0218 –0.0042 –0.0513	0.0204 0.0049 0.0428	–7.6 –1.3	–12.2
(**2**)$_2$·1,4-FIB	CP1 (XB)	0.0174	–0.0190	0.0181	–6.6	–10.5

	CP2 (HB) CP(Pt···Pt)	0.0054 0.0348	–0.0035 –0.0419	0.0041 0.0351	–1.1	
(**3**)$_2$·1,4-FIB I···Pt	CP3 (XB) CP4 (XB) CP(Pt···Pt)	0.0126 0.0087 0.0375	–0.0120 –0.0060 –0.0454	0.0118 0.0084 0.0382	–4.2 –2.1	–8.4
(**3**)$_2$·1,4-FIB I···π	CP3 (XB) CP(Pt···Pt)	0.0133 0.0410	–0.0071 –0.0362	0.0079 0.0304	–2.5	–6.3
1; RORTEZ	CP(Pt···Pt)	0.0307	–0.0373	0.0321	–	–
2; JACTAL	CP(Pt···Pt)	0.0432	–0.0391	0.0327	–	–
3*	CP(Pt···Pt)	0.0340	–0.0420	0.0360	–	–

*For XRD data see the Supporting Information.

In an effort to shed light specifically on the I···Pt^{II} interaction, we performed a Natural Bond Orbital analysis focusing on the second order perturbation analysis, since it is convenient to evaluate donor-acceptor interactions. In **Table 3**, we collected the orbital interactions from Pt^{II} atomic orbitals to the antibonding C–I orbital σ*(C–I) and from the LPs of I to antibonding σ(C–H) orbital. The inspection of these data indicates that the orbital contribution is large for the LP(Pt) → σ*(C–I) in supramolecular dimeric complexes (**1**)$_2$·1,4-FIB, (**1**)·(1,1'-FIDB), and (**2**)$_2$·1,4-FIB and these conclusions are in line to the AIM, MEP, and energetic results. In fact, the orbital contribution is very similar to the binding energies, thus evidencing the importance or orbital donor-acceptor interactions. For (**3**)$_2$·1,4-FIB, the LP(Pt) → σ*(C–I) contribution is smaller (3.80 kcal/mol) in line to the geometry of this complex where the C–I bond is displaced (not pointing directly to the Pt atom). However, in this system there is also an important contribution arising from a σ(Pt–S) → σ*(C–I) electron charge donation, resulting in a concomitant stabilization energy of 3.77 kcal/mol. The orbital contribution of either HB in the rest of complexes, or the F···I interaction in this complex are negligible, thus suggesting that electrostatic effects rather than orbital effects are responsible for those interactions.

Table 3. Orbital donor-acceptor interactions for the adducts at the PBE0/def2-TZVP level of theory. LP, stands for lone pair, σ, σ*, and π* stands for bonding, antibonding sigma-orbital, and antibonding π-orbital respectively.

Supramolecular cluster	Donor	Acceptor	Total $E^{(2)}$ (kcal/mol)	E (PBE0)
(**1**)·(1,1'-FIDB)	LP(Pt) LP(I)	σ*(C–I) σ*(C–H)	11.8 0.29	–12.3
(**1**)$_2$·1,4-FIB	LP(Pt) LP(I)	σ*(C–I) σ*(C–H)	10.2 0.32	–12.2
(**2**)$_2$·1,4-FIB	LP(Pt) LP(I)	σ*(C–I) σ*(C–H)	8.12 0.19	–10.5
(**3**)$_2$·1,4-FIB Pt···I	LP(Pt) σ (Pt–S) LP(F)	σ*(C–I) σ*(C–I) σ*(C–I)	3.80 3.77 0.10	–8.4
(**3**)$_2$·1,4-FIB Pt···π	LP(Pt)	π*(C–C)	3.13	–6.3

Finally, we have also examined orbital donor-acceptor interactions between the Pt atoms in both the adducts and compounds (**Table 4**). A very strong orbital interaction (ranging from 42 to 48 kcal/mol) is found in all adducts between the lone pair at Pt^{II} located at the $5d_{z^2}$ orbital and the empty $6d_z$ orbital of the other Pt^{II} atom (the one that is interacting with the iodine atom). This orbital interaction is significantly smaller in **1**–**3** (**Table 4**) that range from 6 to 18 kcal/mol. Therefore the formation of XB has a strong effect on the $Pt^{II}\cdots Pt^{II}$ interaction.

Table 4. Orbital donor-acceptor interactions for the obtained adducts and parent complexes **1**–**3** at the PBE0/def2-TZVP level of theory. LP and LP* stands for lone pair, and unfilled lone pair orbital, respectively.

Compound	Donor	Acceptor	Total $E^{(2)}$ (kcal/mol)

(**1**)·(1,1'-FIDB)	LP(Pt)	LP*(Pt)	42.4
(**1**)$_2$·1,4-FIB	LP(Pt)	LP*(Pt)	40.6
(**2**)$_2$·1,4-FIB	LP(Pt)	LP*(Pt)	47.4
(**3**)$_2$·1,4-FIB)	LP(Pt)	LP*(Pt)	48.2
(**1**)	LP(Pt)	LP*(Pt)	6.2
(**2**)	LP(Pt)	LP*(Pt)	13.4
(**3**)	LP(Pt)	LP*(Pt)	18.3

Finally, we computed the noncovalent interaction plot (NCIplot) for (**3**)$_2$·1,4-FIB (**Figure 13**); this method is a convenient computation tool to identify which regions in a supramolecular complex interact and to know the attractive or repulsive nature of the interaction. The analysis of the plot indicates a small and green (meaning weak attractive) isosurface between the F and I atoms, thus clearly demonstrating that this interaction also contributes to the stabilization of the assembly. The plot also shows the existence of XB between the I-atom and the Pt^{II} center and that the interaction is extended towards the S and C atoms attached to Pt^{II}. This allows the consideration of the Pt–S and Pt–C bonds as an integrated XB acceptor sites.

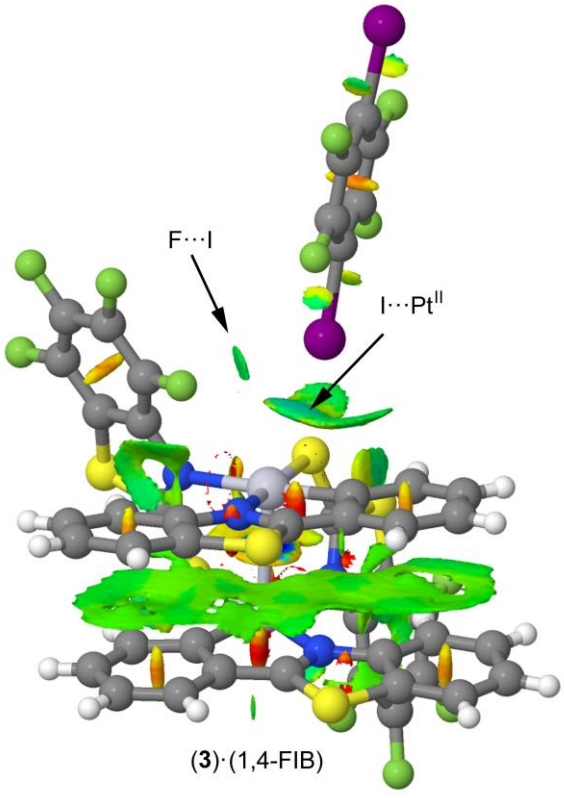

Figure 13. NCI surfaces of (**3**)$_2$·1,4-FIB. The gradient cut-off is s = 0.35 a.u., and the color scale is –0.04 < ρ < 0.04 a.u.

Approaches to identification of the XB in solutions. Interplays between **1**–**3** and the σh donors were studied in solutions by ^{195}Pt NMR, cyclic voltammetry (CV),[65-66] and also by UV-vis.[67] *(i) ^{195}Pt NMR studies.* Although NMR could be used for recognition of XB in the solid state and in solutions, this method is substantially less common than X-ray crystallography as it provides only *collateral* identification of XB by detection the spectral changes between bonded and unbonded forms. In solutions, conventional NMR and chemical shift titration NMR experiments[68] could provide useful information by utilization of XB acceptors featuring NMR-active nuclei such as, for instance, ^{195}Pt. However, ^{195}Pt NMR has never been used for recognition of the I···Pt XB and this work is the first attempt of ^{195}Pt NMR identification of XB involving platinum (II) centers.

Half-lanterns **1**–**3** in CD_2Cl_2 exhibit resonances in the interval between approximately –3800 and –3500 ppm. The addition of the solid 1,4-FIB or 1,1'-FIDB to any one of **1**–**3** in a molar ratio 1:1 had only slight effect on these resonances, while further addition (chemical shift titration was up to 1:20 molar ratio; the maximum ratio was similar to the CV experiment discussed later) led to low field shifts of the ^{195}Pt NMR by 64 (**1**), 18 (**2**), and 1 (**3**) ppm (**Table 5** and **Figures S15–S18**). The addition of 1,1'-FIDB to **1** (molar ratio 1:20) resulted in 20 ppm low field shift of the ^{195}Pt signal. Whilst for **1** and **2** the spectral changes upon the addition of the XB donors are substantial, the spectrum of complex **3** is almost unaffected by treatment with 1,4-FIB. The NMR signal shifts are coherent with the changes of the platinum oxidation anodic peak upon addition of any one of the XB donors to solutions of **1**–**3** (see next subsection).

10.1002/chem.202001196

Table 5. The electrochemical and ^{195}Pt NMR data for **1**–**3** and the corresponding adducts.

Compounds	CV[a]	^{195}Pt NMR[b]
	E, V vs. Fc^+/Fc (Δ)	δ (Δ)
1	E_{pa} 0.07	–3514
1+1,4-FIB	E_{pa} –0.14 (210), E_{pa} 0.50 (425)	–3450 (64)
1+1,1'-FIDB	E_{pa} –0.05 (120) E_{pa} 0.77 (700)	–3494 (20)
2	E_{pa} 0.53	–3783
2+1,4-FIB	E_{pa} 0.80 (270)	–3765 (18)
3	$E_{1/2}$ 0.36	–3573
3+1,4-FIB	$E_{1/2}$ 0.36 (0)	–3571 (2)

[a] Measured in CH_2Cl_2 containing 0.1 *M* [^{n}Bu$_4$N](BF$_4$) at a 50 mVs^{-1} scan rate. The applied potentials were referenced to Fc^+/Fc; at room temperature; [b] Measured in CD_2Cl_2 at room temperature; (Δ) is the difference between the initial value.

(ii) CV. Complexes **1**–**3** undergo electrochemically reversible (**2**; $E_{1/2}$ 0.36 V) or quasi-reversible (E_{pa} 0.53 V for **1**, 0.07 V for **3**) oxidation (vs. Fc^+/Fc) corresponding to the first step (Pt^{II}_2/Pt^{III}_2) of the 2*e*$^-$-oxidation Pt^{II}_2/Pt^{II}_2 to Pt^{III}_2/Pt^{III}_2 accordingly to Ref.[41, 69-72] (**Table 5, Figure S19**).

To study the effect of the added perfluoroarene on the potential, we used 1:20 molar ratios between any one of **1**–**3** and 1,4-FIB (or 1,1'-FIDB) to minimize competitive interactions of the half-lanterns with solvent molecules and also with the supporting electrolyte. Upon the addition of 1,4-FIB and 1,1'-FIDB to a solution of **1** in CH_2Cl_2, the starting curve splits into two oxidation peaks, one with a shift of 200 mV and 120 mV to the cathodic direction and the other one exhibiting 420 mV and 700 mV shift to the anodic area. We assume that these changes may be associated with the linkage of the added XB donor to one of the platinum sites resulting in CT from $d_z^2Pt^{II}$-orbitals to iodine σh. This CT results in the anodic shift of one of the oxidation peaks corresponding to the generation of mixed-valent Pt^{II}–Pt^{III} species.[72]

In contrast to **1**, the electrochemical experiment performed for a mixture of **2** and 1,4-FIB indicates no splitting of the oxidation peak and only its shift to the anodic area (by 270 mV) was detected. Although the quantitative assessment of the effect of added 1,4-FIB is not possible, it is clear that 1,4-FIB provides the overall acceptor effect on **2** and it leads to the increase of the oxidation potential. The addition of XB to a solution of **3** does not lead to any changes of CV.

(iii) UV-vis spectroscopy. All UV-vis spectra of **1**–**3** exhibit a weak low energy band at 450–600 nm assigned, accordingly to Ref.,[73-75] to metal-metal-to-ligand charge transfer (^{1}MMLCT [d(Pt–Pt)→π*(bt)]). The addition of a perfluoroaryl (1:20 molar ratio) to a CH_2Cl_2 solution of **1**–**2** leads to a bathochromic shifts (**1**: 5 nm for both 1,4-FIB and 1,1'-FIDB; **2**: 38 nm for 1,4-FIB; no changes were detected upon addition of 1,4-FIB to **2**) of the ^{1}MMLCT absorption band (the Supporting Information). A similar red shifts have been observed upon interaction of the half-lanterns via their d_z^2-Pt_2^{II} orbitals with Ag^+, Cd^{2+}, Pb^{2+}, Hg^{2+} acting as Lewis acids.[76-78] In line with these results, the red shifts observed in this work may be accounted for by CT from d_z^2-LP at the Pt^{II} atom to iodine σh in the XB bound adducts (**Table 54** and **Figure S14**).

Our solution studies for mixtures of **1**–**2** and 1,4-FIB uncovered in *i*–*iii* favor the preservation of XB in $CH(D)_2Cl_2$ solutions, although excess 1,4-FIB is required. The association in solution was not detected for **3**, which exhibits the lowest Lewis basicity as follows from our MEP calculations.

Conclusions

Half-lantern complexes **1**–**3** (**Figure 1**), exhibiting an increased nucleophilicity of the outer d_z^2-orbitals of $(Pt^{II})_2$ centers, interact with symmetric bifunctional halogen bond donors 1,4-FIB and 1,1'-FIDB (**Figure 2**) to give solid (**1**–**3**)$_2$·1,4-FIB and infinite polymeric [**1**·1,1'-

FIDB]$_n$ adducts (**Figure 6**). The assembly was achieved via (Aryl)I···d_z^2[Pt^{II}] halogen bond between iodine σ-holes and lone pairs of the positively charged (Pt^{II})$_2$ centers, acting as nucleophilic sites. We revealed that the halogen bond interaction between Pt^{II} and two σ-hole-XB donors is moderately strong and dominated by orbital donor-acceptor interactions between the d_z^2-lone pair at the Pt^{II} atom and the antibonding σ*(C–I) orbital. The ^{195}Pt NMR titration, UV-vis spectroscopy studies, and cyclic voltammetry data for (**1**–**2**)$_2$·1,4-FIB indicate that the halogen bonding is preserved in CH(D)$_2$Cl$_2$ solutions, although excess 1,4-FIB is required.

Recognized cases of metal-involving halogen bond are quite rare and only simple 1:1 adducts of halogen bond donors with metal centers, featuring an expressed Lewis basicity, were reported. At the same time, assembly or supramolecular design via R^{EWG}X···d_z^2[M] halogen bonding has never been conducted and this work provides the first example of utilization of halogen···metal noncovalent interactions for construction of supramolecular architectures.

ACKNOWLEDGMENTS

Support of the synthetic work and compound characterizations from the Russian Foundation for Basic Research (grant 18-29-04006) is gratefully acknowledged. Electrochemical part of this work was supported by the Russian Foundation for Basic Research project 19-29-08026. E.A.K. is thankful to the Saint Petersburg State University for postdoctoral fellowship. Physicochemical studies were performed at the Center for Magnetic Resonance, Center for X-ray Diffraction Studies, and Center for Chemical Analysis and Materials Research (all belonging to Saint Petersburg State University). V.Y.K. is grateful to South Ural State University (Act 211 Government of the Russian Federation, contract No 02.A03.21.0011) for putting facilities at his disposal. We are indebted to Prof. Dr. P.M. Tolstoy and Dr. D.M. Ivanov for valuable suggestions and Dr. A.V. Rozhkov for kind loan of 1,1'-FIDB and 2-mercapto-4,5,6,7-tetrafluorobenzothiazole.

10.1002/chem.202001196

Keywords: halogen bonding, assembly, supramolecular chemistry, cyclometalated complex, platinum, theoretical calculations

References

[1] S. K. Seth, A. Bauza, A. Frontera, in *Understanding Intermolecular Interactions in the Solid State: Approaches and Techniques, Vol. 26* (Ed.: D. Chopra), **2019**, pp. 285-333.
[2] P. Politzer, J. Murray, *Crystals* **2019**, *9*, 165.
[3] L. Brammer, *Faraday Discussions* **2017**, *203*, 485-507.
[4] G. Cavallo, P. Metrangolo, R. Milani, T. Pilati, A. Priimagi, G. Resnati, G. Terraneo, *Chemical Reviews* **2016**, *116*, 2478-2601.
[5] B. Li, S.-Q. Zang, L.-Y. Wang, T. C. W. Mak, *Coordination Chemistry Reviews* **2016**, *308*, 1-21.
[6] A. M. Maharramov, K. T. Mahmudov, M. N. Kopylovich, A. J. Pombeiro, *Non-covalent interactions in the synthesis and design of new compounds*, Wiley Online Library, **2016**.
[7] R. Tepper, U. S. Schubert, *Angewandte Chemie-International Edition* **2018**, *57*, 6004-6016.
[8] J. Y. C. Lim, P. D. Beer, *Chem* **2018**, *4*, 731-783.
[9] S. Scheiner, M. Michalczyk, W. Zierkiewicz, *Coordination Chemistry Reviews* **2020**, *405*, 213136.
[10] K. T. Mahmudov, A. V. Gurbanov, F. I. Guseinov, M. F. C. Guedes da Silva, *Coordination Chemistry Reviews* **2019**, *387*, 32-46.
[11] K. T. Mahmudov, S. Arimitsu, J. M. Saá, Y. Sarazin, A. Frontera, S. Yamada, A.-M. Caminade, S. H. Chikkali, P. Mal, N. Momiyama, *Noncovalent Interactions in Catalysis*, Royal Society of Chemistry, **2019**.
[12] P. Nagorny, Z. K. Sun, *Beilstein Journal of Organic Chemistry* **2016**, *12*, 2834-2848.
[13] D. Bulfield, S. M. Huber, *Chemistry-a European Journal* **2016**, *22*, 14434-14450.
[14] S. Benz, A. I. Poblador-Bahamonde, N. Low-Ders, S. Matile, *Angewandte Chemie-International Edition* **2018**, *57*, 5408-5412.
[15] M. Breugst, D. von der Heiden, J. Schmauck, *Synthesis-Stuttgart* **2017**, *49*, 3224-3236.
[16] K. T. Mahmudov, M. N. Kopylovich, M. F. C. Guedes da Silva, A. J. L. Pombeiro, *Coordination Chemistry Reviews* **2017**, *345*, 54-72.
[17] G. Berger, J. Soubhye, F. Meyer, *Polymer Chemistry* **2015**, *6*, 3559-3580.
[18] L. Mendez, G. Henriquez, S. Sirimulla, M. Narayan, *Molecules* **2017**, *22*.
[19] P. S. Ho, *Future Medicinal Chemistry* **2017**, *9*, 637-640.
[20] A. Dalpiaz, B. Pavan, V. Ferretti, *Drug Discovery Today* **2017**, *22*, 1134-1138.
[21] Y. X. Lu, Y. T. Liu, Z. J. Xu, H. Y. Li, H. L. Liu, W. L. Zhu, *Expert Opinion on Drug Discovery* **2012**, *7*, 375-383.
[22] C. A. Bayse, *New Journal of Chemistry* **2018**, *42*, 10623-10632.
[23] A. M. S. Riel, R. K. Rowe, E. N. Ho, A.-C. C. Carlsson, A. K. Rappé, O. B. Berryman, P. S. Ho, *Accounts of Chemical Research* **2019**, *52*, 2870-2880.
[24] C. B. Aakeroy, K. R. Seddon, *Chem. Soc. Rev.* **1993**, *22*, 397-407.
[25] W. Z. Wang, B. M. Ji, Y. Zhang, *J. Phys. Chem. A* **2009**, *113*, 8132-8135.
[26] K. T. Mahmudov, M. N. Kopylovich, M. F. C. Guedes da Silva, A. J. L. Pombeiro, *Dalton Transactions* **2017**, *46*, 10121-10138.
[27] P. Scilabra, G. Terraneo, G. Resnati, *Accounts of Chemical Research* **2019**, *52*, 1313-1324.
[28] S. J. Grabowski, I. Alkorta, J. Elguero, *The Journal of Physical Chemistry A* **2013**, *117*, 3243-3251.
[29] M. J. Katz, K. Sakai, D. B. Leznoff, *Chem. Soc. Rev.* **2008**, *37*, 1884-1895.
[30] C. Janiak, *Journal of the Chemical Society-Dalton Transactions* **2000**, 3885-3896.
[31] D. M. Ivanov, A. S. Novikov, I. V. Ananyev, Y. V. Kirina, V. Y. Kukushkin, *Chemical Communications* **2016**, *52*, 5565-5568.
[32] S. V. Baykov, U. Dabranskaya, D. M. Ivanov, A. S. Novikov, V. P. Boyarskiy, *Crystal Growth & Design* **2018**, *18*, 5973-5980.
[33] U. Dabranskaya, D. M. Ivanov, A. S. Novikov, Y. V. Matveychuk, N. A. Bokach, V. Y. Kukushkin, *Crystal Growth & Design* **2018**, *19*, 1364-1376.
[34] D. W. Shaffer, S. A. Ryken, R. A. Zarkesh, A. F. Heyduk, *Inorganic Chemistry* **2012**, *51*, 12122-12131.
[35] Y. Yamashina, Y. Kataoka, Y. Ura, *European Journal of Inorganic Chemistry* **2014**, 4073-4078.
[36] R. A. Gossage, A. D. Ryabov, A. L. Spek, D. J. Stufkens, J. A. M. van Beek, R. van Eldik, G. van Koten, *Journal of the American Chemical Society* **1999**, *121*, 2488-2497.
[37] M. Chaaban, C. Zhou, H. Lin, B. Chyi, B. Ma, *Journal of Materials Chemistry C* **2019**, *7*, 5910-5924.
[38] M. Yoshida, M. Kato, *Coordination Chemistry Reviews* **2018**, *355*, 101-115.

[39] A. A. Eliseeva, D. M. Ivanov, A. S. Novikov, V. Y. Kukushkin, *Crystengcomm* **2019**, *21*, 616-628.
[40] A. S. Novikov, D. M. Ivanov, Z. M. Bikbaeva, N. A. Bokach, V. Y. Kukushkin, *Crystal Growth & Design* **2018**, *18*, 7641-7654.
[41] E. A. Katlenok, A. A. Zolotarev, A. Y. Ivanov, S. N. Smirnov, K. P. Balashev, *Journal of Structural Chemistry* **2015**, *56*, 880-886.
[42] V. Sicilia, M. Baya, P. Borja, A. Martin, *Inorg Chem* **2015**, *54*, 7316-7324.
[43] D. M. L. Goodgame, R. W. Rollins, A. C. Skapski, in *Inorganica Chimica Acta, Vol. 83*, **1984**, pp. L11-L12.
[44] T. Koshiyama, M. Kato, *Acta Crystallogr C* **2005**, *61*, m173-176.
[45] M. J. Romero, A. Rodríguez, A. Fernández, M. López-Torres, D. Vázquez-García, J. M. Vila, J. J. Fernández, *Polyhedron* **2011**, *30*, 2444-2450.
[46] A. Osamu, U. Keisuke, T. Kiyoshi, Y. Shingo, S. Yoichi, O. Masayoshi, *Bulletin of the Chemical Society of Japan* **2003**, *76*, 549-555.
[47] B. Ma, P. I. Djurovich, S. Garon, B. Alleyne, M. E. Thompson, *Advanced Functional Materials* **2006**, *16*, 2438-2446.
[48] M. Maryam Sadat, S. Akbar Raissi, A. Vahid, *Phosphorus, Sulfur, and Silicon and the Related Elements*, *193*, 415-422.
[49] V. Sicilia, J. Forniés, J. M. Casas, A. Martín, J. A. López, C. Larraz, P. Borja, C. Ovejero, D. Tordera, H. Bolink, *Inorganic Chemistry* **2012**, *51*, 3427-3435.
[50] P. Politzer, J. S. Murray, *Journal of Computational Chemistry* **2018**, *39*, 464-471.
[51] G. R. Desiraju, P. S. Ho, L. Kloo, A. C. Legon, R. Marquardt, P. Metrangolo, P. Politzer, G. Resnati, K. Rissanen, *Pure and Applied Chemistry,* **2013**, *18*, 1711-1713.
[52] R. S. Rowland, R. Taylor, *The Journal of Physical Chemistry* **1996**, *100*, 7384-7391.
[53] E. Bartashevich, S. Mukhitdinova, I. Yushina, V. Tsirelson, *Acta Crystallographica Section B* **2019**, *75*, 117-126.
[54] C. B. Aakeroy, D. L. Bryce, G. R. Desiraju, A. Frontera, A. C. Legon, F. Nicotra, K. Rissanen, S. Scheiner, G. Terraneo, P. Metrangolo, G. Resnati, *Pure and Applied Chemistry,* **2019**, *91*, 1889-1892.
[55] M. A. Kinzhalov, A. A. Eremina, D. M. Ivanov, A. S. Novikov, E. A. Katlenok, K. P. Balashev, V. V. Suslonov, *Zeitschrift für Kristallographie - Crystalline Materials,* **2017**, 232, 797-805.
[56] M. A. Spackman, D. Jayatilaka, *CrystEngComm* **2009**, *11*, 19-32.
[57] A. A. Eliseeva, D. M. Ivanov, A. S. Novikov, A. V. Rozhkov, I. V. Kornyakov, A. Y. Dubovtsev, V. Y. Kukushkin, *Dalton Transactions* **2020**, *49*, 356-367.
[58] R. O. Fuller, C. S. Griffith, G. A. Koutsantonis, K. M. Lapere, B. W. Skelton, M. A. Spackman, A. H. White, D. A. Wild, *CrystEngComm* **2012**, *14*, 804-811.
[59] J. J. McKinnon, D. Jayatilaka, M. A. Spackman, *Chemical Communications* **2007**, 3814-3816.
[60] S. L. Tan, M. M. Jotani, E. R. T. Tiekink, *Acta Crystallographica Section E* **2019**, *75*, 308-318.
[61] C. B. Pinto, L. H. R. Dos Santos, B. L. Rodrigues, *Acta Crystallographica Section C* **2019**, *75*, 707-716.
[62] J. J. McKinnon, M. A. Spackman, A. S. Mitchell, *Acta Crystallographica Section B* **2004**, *60*, 627-668.
[63] E. Espinosa, E. Molins, C. Lecomte, *Chemical Physics Letters* **1998**, *285*, 170-173.
[64] A. Bauzá, A. Frontera, *ChemPhysChem* **2020**, *21*, 26-31.
[65] G. Creste, S. Groni, C. Fave, M. Branca, B. Schöllhorn, *Faraday Discussions* **2017**, *203*, 301-313.
[66] C. Fave, B. Schöllhorn, *Current Opinion in Electrochemistry* **2019**, *15*, 89-96.
[67] M. Erdélyi, *Chem. Soc. Rev.* **2012**, *41*, 3547-3557.
[68] D. von der Heiden, A. Vanderkooy, M. Erdélyi, *Coordination Chemistry Reviews* **2020**, *407*, 213147.
[69] Y. Zhu, K. Luo, L. Zhao, H. Ni, Q. Li, *Dyes and Pigments* **2017**, *145*, 144-151.
[70] A. Rie, K. Atsushi, C. Ho-Chol, K. Masako, *Bulletin of the Chemical Society of Japan* **2011**, *84*, 218-225.
[71] Z. Wang, L. Jiang, Z.-P. Liu, C. R. R. Gan, Z. Liu, X.-H. Zhang, J. Zhao, T. S. A. Hor, *Dalton Transactions* **2012**, *41*, 12568-12576.
[72] M. Yoshida, N. Yashiro, H. Shitama, A. Kobayashi, M. Kato, *Chemistry – A European Journal* **2016**, *22*, 491-495.
[73] R. Aoki, A. Kobayashi, H.-C. Chang, M. Kato, *Bulletin of the Chemical Society of Japan* **2011**, *84*, 218-225.
[74] V. Sicilia, P. Borja, J. M. Casas, S. Fuertes, A. Martín, *Journal of Organometallic Chemistry* **2013**, *731*, 10-17.

[75] A. Chakraborty, J. E. Yarnell, R. D. Sommer, S. Roy, F. N. Castellano, *Inorganic Chemistry* **2018**, *57*, 1298-1310.
[76] D. P. Bender, J. K. Nagle, *Inorganica Chimica Acta* **1994**, *225*, 201-205.
[77] V. Sicilia, P. Borja, M. Baya, J. M. Casas, *Dalton Transactions* **2015**, *44*, 6936-6943.
[78] M. V. Nikolaeva, E. A. Katlenok, M. S. Khakhalina, M. V. Puzyk, K. P. Balashev, *Journal of Physics: Conference Series* **2015**, *643*, 012045.

10.1002/chem.202001196

Entry for the Table of Contents

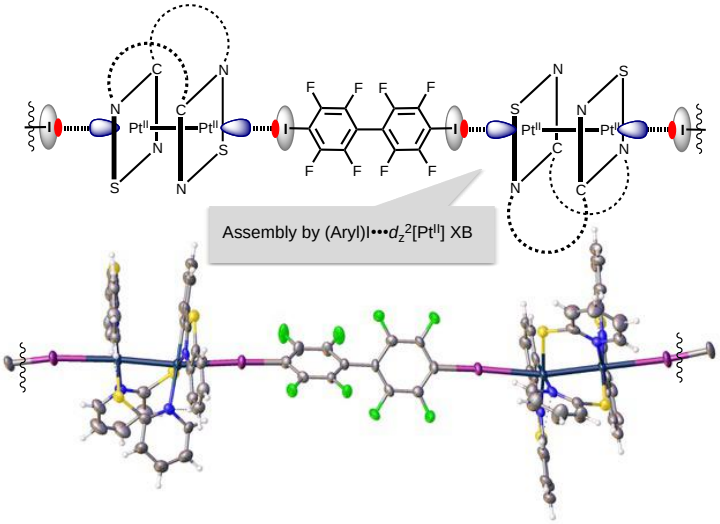

Half-lantern d_z^2[Pt$^{II}_2$] complexes, where Pt$^{II}_2$ center exhibits an increased nucleophilicity of the outer orbitals (proved by DFT calculations) were assembled with symmetric XB donating diiodoperfluoroarenes to give extended supramolecular arrays formed via (Aryl)I•••d_z^2[Pt^{II}] XB that was studied by XRD and supported by extensive theoretical calculations. The CV, ^{195}Pt NMR, and UV-vis studies provide evidences that the XB is preserved in solutions.